THE JOURNAL OF BIOLOGICAL CHEMISTRY
Vol. 280, No. 25, Issue of June 24, pp. 24072–24084, 2005

Printed in U.S.A.

Spatial and Functional Heterogeneity of Sphingolipid-rich Membrane Domains*

Received for publication, February 28, 2005, and in revised form, April 18, 2005
Published, JBC Papers in Press, April 19, 2005, DOI 10.1074/jbc.M502244200

Etsuko Kiyokawa‡§¶, Takeshi Baba‖, Naomi Otsuka‡, Asami Makino‡, Shinichi Ohno‖, and Toshihide Kobayashi‡‡‡**

*From ‡RIKEN, Wako, Saitama 351-0198, Japan, §Precursory Research for Embryonic Science and Technology (PRESTO), Japan Science and Technology Agency, Kawaguchi, Saitama 332-0012, Japan, ‖Department of Anatomy, Interdisciplinary Graduate School of Medicine and Engineering, University of Yamanashi, Yamanashi 409-3898, Japan, and **INSERM U585, Institut National des Sciences Appliquées-Lyon, 69621 Villeurbanne, France*

Little is known about the organization of lipids in biomembranes. Lipid rafts are defined as sphingolipid- and cholesterol-rich clusters in the membrane. Details of the lipid distribution of lipid rafts are not well characterized mainly because of a lack of appropriate probes. Ganglioside GM1-specific protein, cholera toxin, has long been the only lipid probe of lipid rafts. Recently it was shown that earthworm toxin, lysenin, specifically recognizes sphingomyelin-rich membrane domains. Binding of lysenin to sphingomyelin is accompanied by the oligomerization of the toxin that leads to pore formation in the target membrane. In this study, we generated a truncated lysenin mutant that does not oligomerize and thus is non-toxic. Using this mutant lysenin, we showed that plasma membrane sphingomyelin-rich domains are spatially distinct from ganglioside GM1-rich membrane domains in Jurkat T cells. Like T cell receptor activation and cross-linking of GM1, cross-linking of sphingomyelin induced calcium influx and ERK phosphorylation in the cell. However, unlike CD3 or GM1, cross-linking of sphingomyelin did not induce significant protein tyrosine phosphorylation. Combination of lysenin and sphingomyelinase treatment suggested the involvement of G-protein-coupled receptor in sphingomyelin-mediated signal transduction. These results thus suggest that the sphingomyelin-rich domain provides a functional signal cascade platform that is distinct from those provided by T cell receptor or GM1. Our study therefore elucidates the spatial and functional heterogeneity of lipid rafts.

Whereas the bilayer organization of biomembranes can be reconstituted in artificial liposomes with a simple lipid composition, biological membranes contain thousands of different lipid species whose cellular distribution is stringently controlled (1). This complex distribution of lipids suggests that the targeting of lipids is highly regulated and that cells require a complex lipid supramolecular organization within their membranes. In the plasma membrane, most of the sphingolipids reside in the outer leaflet, whereas phospholipids containing the amino groups, phosphatidylethanolamine and phosphatidylserine, are located in the cytoplasmic surface (2, 3). Lateral segregation of lipids on the plasma membrane is also reported. A typical example is a lipid heterogeneity between the apical and the basolateral membranes of epithelial cells (4). The lipid diffusion barrier between axons and dendrites (5, 6) is another example.

The existence of submicrometer scale heterogeneity of plasma membrane lipids is a matter of debate. In particular, the proposed existence of specific types of microdomains called lipid rafts that are enriched in cholesterol and sphingolipids attracts much attention (7, 8). Lipid rafts are suggested to play important roles in a number of cellular processes as diverse as signal transduction, membrane traffic, and pathogen entry (9). Detergent insolubility has been an operational definition of lipid rafts in cell membranes (10). However, recent results indicate that detergent resistance does not correlate with the existence of lipid domains (11). Therefore, a more direct approach is required to understand the detailed organization of membrane lipids. At present, this approach is hindered by the lack of appropriate probes.

Sphingomyelin (SM)[1] is a major sphingolipid of mammalian

* This work was supported by grants from the RIKEN Frontier Research System (to T. K.), the Bioarchitect Research Project of RIKEN (to T. K.), the RIKEN presidential research grant for intersystem collaboration (to E. K. and T. K.), grants from the Ministry of Education, Science, Sports and Culture of Japan (Grants 13770119 (to E. K.), 15590157 (to T. B.), and 14370753 and 16044247 (to T. K.)), the RIKEN presidential research grant for innovative tool development (to E. K.), the Hayashi Memorial Foundation for Female Natural Scientists (to E. K.), the Novartis Foundation (Japan) for the Promotion of Science (to E. K.), and the Ara Parseghian Medical Research Foundation (to T. K.). The costs of publication of this article were defrayed in part by the payment of page charges. This article must therefore be hereby marked "*advertisement*" in accordance with 18 U.S.C. Section 1734 solely to indicate this fact.

¶ To whom correspondence may be addressed: Dept. of Tumor Virology, Research Inst. for Microbial Diseases, Osaka University, 3-1, Yamada-oka, Suita-shi, Osaka 565-0871, Japan. E-mail: kiyokawa@biken.osaka-u.ac.jp.

‡‡ To whom correspondence may be addressed: RIKEN, 2-1 Hirosawa, Wako, Saitama 351-0198, Japan. Tel.: 81-48-467-9612; Fax: 81-48-467-8693; E-mail: kobayasi@riken.jp.

[1] The abbreviations used are: SM, sphingomyelin; Chol, cholesterol; CTxB, cholera toxin B subunit; ERK, extracellular signal-regulated kinase; LAT, linker for activated T cells; LPA, lysophosphatidic acid; MBP, maltose-binding protein; *N*-NBD-PE, 1,2-dioleoyl-*sn*-glycero-3-phosphoethanolamine-*N*-(7-nitro-2–1,3-benzoxadiazol-4-yl); NPA, Niemann-Pick type A; PC, phosphatidylcholine; SMase, sphingomyelinase; S1P, sphingosine 1-phosphate; TCR, T cell receptor; GM1, Galβ1,3GalNAcβ1,4(Neu5Acα2,3)Galβ1,4Glcβ1,1′-ceramide; GM2, GalNAcβ1,4(Neu5Acα2,3)Galβ1,4Glcβ1,1′-ceramide; GST, glutathione *S*-transferase; MTT, 3-(4,5-dimethylthiazol-2-yl)-2,5-diphenyltetrazolium bromide; PKC, protein kinase C; PMA, phorbol 12-myristate-13-acetate; NT-Lys, non-toxic lysenin; HV-NT-Lys, His-Venus-non-toxic lysenin; HmV-NT-Lys, His-monomer Venus A206K-non-toxic lysenin; mRFP, monomeric red fluorescent protein; HmRFP-NT-Lys, His-mRFP-NT-Lys; ELISA, enzyme-linked immunosorbent assay; PBS, phosphate-buffered saline; FACS, fluorescence-activated cell sorter; EM, electron micrograph; AM, acetoxymethyl ester; GFP, green fluorescent protein; PLC, phospholipase C; MAPK, mitogen-activated protein kinase; MEK, MAPK/ERK kinase; MAPKK, MAPK kinase; MAPKKK, MAPK kinase kinase.

cells. Previously it was shown that the earthworm toxin lysenin specifically recognizes SM (12–14). Recently we have revealed that lysenin recognizes SM only when SM forms aggregates or domains (15, 16). Using these characteristics, we have shown that SM exists as aggregates of at least a few lipid molecules in most of the membranes. We have also shown that the distribution of SM is different among different cell types as well as between different membrane domains in the same cell. One big problem of using lysenin as an SM probe is its toxicity. In the present study, we developed a non-toxic mutant of lysenin that recognizes SM. This mutant lysenin made it possible to examine the distribution of SM in living cells. Using mutant lysenin and sphingomyelinase, we showed that SM-rich domains in the plasma membrane are spatially and functionally segregated from the ganglioside GM1-rich membrane domains.

MATERIALS AND METHODS

Antibodies and Reagents—Anti-maltose-binding protein (MBP) antisera, pC2X vector, and amylose resin were purchased from New England Biolabs. Polyclonal anti-glutathione *S*-transferase (GST) antibody, pGEX vectors, and GST-Sepharose 4B were purchased from Roche Applied Science. Monoclonal antibody against GST was a gift from Dr. A. Kojima (17) (National Institute of Infectious Diseases, Japan). Alexa Fluor™ 488-conjugated antibody was prepared using a protein labeling kit (Molecular Probes). Sheep anti-mouse immunoglobulin and goat anti-choleragenoid (cholera toxin B subunit) were from Chemicon and List Biological Laboratories, respectively. Secondary antibodies and cholera toxin B subunit (CTxB) conjugated with various Alexa Fluor fluorophores were from Molecular Probes. Sphingomyelinase (SMase) from *Bacillus cereus* was purchased from Higetashoyu and Sigma. CTxB, 3-(4,5-dimethylthiazol-2-yl)-2,5-diphenyltetrazolium bromide (MTT), and lysophosphatidic acid (LPA) were from Sigma. Anti-pan-ERK and -protein kinase C (PKC) antibodies were purchased from BD Transduction Laboratories. Anti-linker for activated T cells (LAT) and phosphospecific antibodies were from Cell Signaling Technology Inc. Anti-CD3 antibody was from Pharmingen. 1,2-Dioleoyl-*sn*-glycero-3-phosphoethanolamine-*N*-(7-nitro-2–1,3-benzoxadiazol-4-yl) (*N*-NBD-PE), brain SM, egg phosphatidylcholine (PC), liver phosphatidylethanolamine, brain phosphatidylserine, liver phosphatidylinositol, phosphatidic acid, brain ceramide, and brain cerebroside were purchased from Avanti Polar Lipids. Sphingosine, D-*erythro*-sphingosine 1-phosphate, and sphingosylphosphorylcholine were from Biomol Research Laboratories, Inc. PD98059 was from Promega. U73122 and phorbol 12-myristate-13-acetate (PMA) were from Calbiochem.

Expression and Isolation of Recombinant Lysenins—The cDNA of lysenin and polyclonal anti-lysenin antibody were generous gifts from Drs. Y. Sekizawa and H. Kobayashi of Zenyaku Kogyo Inc. (18). The cDNA fragments were amplified by PCR and subcloned into pC2X or pGEX-4T. The recombinant proteins fused to MBP or GST were expressed in *Escherichia coli* JM 109 or BL 21, purified using amylose resin or GST-Sepharose 4B according to the manufacturer's instructions. For deletion mutants, forward primers containing BamHI site and reverse primers containing a HindIII site were used for PCR, and the obtained fragments were cloned into pC2X or pGEX after digesting with the corresponding enzymes. Amplified cDNA sequences from wild type and mutants were confirmed using BigDye Terminator and Genetic Analyzer ABI Prism™ 310 (PE Applied Biosystems). pRSET-Venus was a gift from T. Nagai and A. Miyawaki (RIKEN) (19). To obtain recombinant His-Venus-non toxic lysenin (HV-NT-Lys), a PCR-amplified cDNA fragment corresponding to amino acids 161–297 was inserted into the 3′ terminus of the Venus sequence. The monomer Venus was prepared by replacing amino acid Ala-206 with Lys as described previously (20). His-tagged proteins were expressed in *E. coli* and lysed and purified by AKTAprime (Amersham Biosciences) according to the manufacturer's protocol.

Enzyme-linked Immunosorbent Assay (ELISA)—ELISA was performed as described previously (21).

Kinetic Analysis of GST-Non-toxic Lysenin (NT-Lys) Binding to SM—Binding of GST-NT-Lys to SM was quantified using a BIAcore™ system instrument (Pharmacia Biosensor AB) as described previously (12).

Liposome Binding Assay—Multilamellar liposomes were prepared as described previously (12, 13) and incubated with recombinant proteins at 37 °C for 30 min. 0.5 ml of the suspension was mixed with 1 ml of 2.1 M sucrose in 10 mM Hepes (pH 7.2), loaded at the bottom of an ultracentrifuge tube, and overlaid sequentially with 1.5 ml of 1.2 M sucrose and 1 ml of 0.8 M sucrose. The gradient was centrifuged for 20 h at 90,000 × *g* at 4 °C using a Beckman Coulter Optima™ MAX-E ultracentrifuge. Fractions (0.6 ml each) were collected from the top of the tube and were subjected to Western blotting. Fluorescence intensity of *N*-NBD-PE was also measured to monitor the position of liposomes in the gradient.

Cells and Cell Culture—Niemann-Pick type A (NPA) fibroblasts and the Jurkat cell line were gifts from Drs. Hitoshi Sakuraba and Michiyuki Matsuda, respectively. NPA cells were maintained in Ham's F-10 medium plus 10% fetal bovine serum (Invitrogen) and penicillin/streptomycin. The mutant Jurkat cell lines were purchased from ATCC. The wild type and mutant Jurkat cell lines were maintained in RPMI 1640 medium (Sigma) supplemented with 10% fetal bovine serum and penicillin/streptomycin.

Immunofluorescence—NPA fibroblasts were plated onto cover glass. After 24–48 h, cells were fixed with 4% paraformaldehyde in phosphate-buffered saline (PBS) for 20 min, permeabilized with 50 μg/ml digitonin for 10 min, preincubated with 0.2% gelatin in PBS for 20 min at room temperature, and then incubated with the recombinant protein for 60 min at 4 °C. Cells were fixed again, incubated with anti-GST antibody for 30 min followed by the addition of anti-rabbit antibody conjugated to Alexa 488, and mounted in Mowiol. For SMase treatment, NPA cells were incubated with 10 milliunits/ml recombinant *B. cereus* sphingomyelinase in PBS for 1 h at 37 °C.

Jurkat cells were incubated with 50 μg/ml HV-NT-Lys or His-monomer Venus A206K-non-toxic lysenin (HmV-NT-Lys) in the presence of 10 μg/ml CTxB conjugated with Alexa 594 on ice for 30 min. Cells were washed with PBS and resuspended in Opti-MEM (Invitrogen). Cells were then placed onto a glass-bottomed culture dish precoated with poly-L-lysine (MatTEK). Confocal images were obtained using an LSM510 confocal microscope equipped with Plan-Apochromat 100× (1.4 numerical aperture) objective and processed with LSM Image Browser (Zeiss).

MTT Assay—Cell viability was assessed by the MTT assay (22). 1×10^6 Jurkat cells were washed with PBS twice, incubated with various concentrations of GST or GST-NT-Lys for 30 min at room temperature, resuspended in RPMI 1640 medium without sera, and then cultured in the presence of 0.5 mg/ml MTT at 37 °C. After 4 h of incubation, MTT solution was removed, and cells were disrupted with Me_2SO. The absorbance at 595 nm was measured with a spectrophotometer.

Fluorescence-activated Cell Sorter (FACS) Analysis—In Fig. 2, 1×10^6 Jurkat cells were washed twice with PBS, incubated with 50 μg/ml GST or GST-NT-Lys for 30 min at room temperature, washed, and further incubated with or without 10 μg/ml monoclonal anti-GST antibody followed by goat anti-mouse IgG antibody conjugated with Alexa 488. In Fig. 3, cells were labeled with Alexa 488-conjugated CTxB, HmV-NT-Lys, or His-mRFP-NT-Lys (HmRFP-NT-Lys) at 4 °C to avoid rapid internalization of CTxB. HmRFP-NT-Lys was prepared from monomeric red fluorescent protein (mRFP) (23), and specific binding to SM was confirmed (data not shown). Flow cytometry was performed on a Beckman Coulter EPICS XL. Data analyses were performed using the software package EXPO32.

Electron Microscopy—Plasma membrane was prepared from Jurkat cells as described previously (24, 25). Briefly cells were first labeled with HmV-NT-Lys and biotinylated cholera toxin B fragments at 4 °C and then fixed with 4% paraformaldehyde and 0.02% glutaraldehyde for 10 min at 4 °C. The fixed cells were quenched with 0.1 M NH_4Cl and blocked with 2% bovine serum albumin. The fixed cells were labeled with anti-GFP rabbit polyclonal antibody at 4 °C followed by labeling with goat anti-rabbit IgG-5-nm gold and goat anti-biotin-IgG-10-nm gold at 4 °C. The labeled cells were attached to nickel EM grids that had been coated with Formvar and carbon and treated with poly-L-lysine (0.8 mg/ml for 30 min followed by a 10-s distilled H_2O rinse and air drying). The cell-attached EM grids were covered with a poly-L-lysine-coated coverslip, and pressure was applied to the coverslip for 20 s by bearing down with a rubber cork. The coverslips were lifted, leaving fragments of the cell membranes adherent to the grids. Membranes were fixed in 2% glutaraldehyde for 10 min and further fixed for 10 min with 1% OsO_4 in distilled H_2O. Samples were then processed for 10 min in 1% aqueous tannic acid followed by two 5-min rinses with distilled H_2O, 10 min with 1% aqueous uranyl acetate, and two 1-min rinses with distilled H_2O. The grids were air-dried, examined, and photographed at ×50,000 using a Hitachi H-7500 transmission electron microscope (Hitachi, Tokyo, Japan) at 80 kV.

Image Analysis—Twenty EM negatives were digitized with an image scanner (Epson GT-X700). The scanned images were contrast-adjusted and trimmed at 1500 × 1500 nm with Photoshop 6.0 software. The *x*-*y* coordinates of each gold particle were obtained with ImageJ public

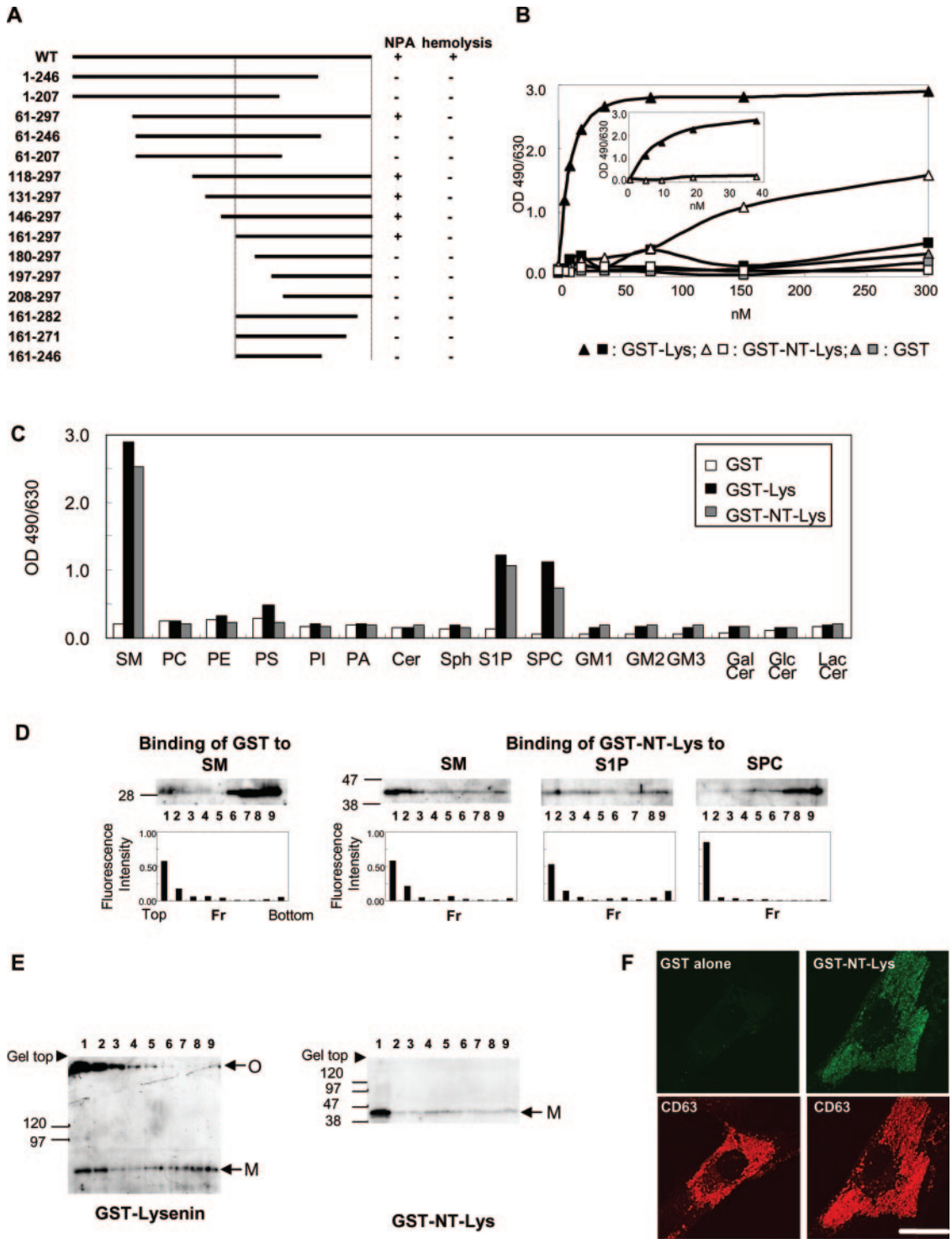

FIG. 1. **Characterization of non-toxic probe for SM.** *A*, schematic representation of deletion mutants of lysenin. Wild type (*WT*) and the number of amino acids of lysenin coded by mutants are indicated at the *left*. The *bars* corresponding to mutants are indicated in the *middle*. NPA cells were incubated at a concentration of 10 μg/ml for wild type and 50 μg/ml for mutant lysenins. Positive (+) or negative (−) labeling of NPA cells with these mutants is indicated at the *right side* of the *lines*. Positive (+) or negative (−) hemolytic activities of these mutant proteins at a concentration of 50 μg/ml are indicated at the *right*. *B* and *C*, binding of GST-tagged lysenin and GST-NT-Lys to various lipids measured by ELISA. The microtiter wells were coated with 50 μl of a 10 μM concentration of various lipids. Wells were then incubated with 100 μl of various concentrations of GST-tagged wild type lysenin, GST-NT-Lys, or GST (*B*) or 100 μl of 10 μg/ml GST-tagged wild type lysenin or 25 μg/ml GST-NT-Lys or GST (*C*). After washing, the wells were further incubated with anti-GST antibody and the corresponding secondary antibody conjugated with biotin. The binding of the secondary antibody was detected at 490 nm as signal and 630 nm as reference (21). 300 nM protein corresponds to 20 μg/ml GST-Lys, 13 μg/ml GST-NT-Lys, and 7.8 μg/ml GST. *PE*, phosphatidylethanolamine; *PS*, phosphatidylserine; *PI*, phosphatidylinositol; *PA*, phosphatidic acid; *Cer*, ceramide; *Sph*, sphingosine; *SPC*, sphingosylphosphorylcholine; *GalCer*, galactosylceramide; *GlcCer*, glucosylceramide; *LacCer*, lactosylceramide; *GM3*, NeuAcα2,3Galβ1,4Glcβ1,1′-ceramide. In *B*, *triangles* show binding to SM, and *squares* indicate binding to PC. *Inset* in *B* shows the expansion of the area of the curve between 0 and 40 nM. *D*, binding of GST-tagged truncated lysenin to liposomes containing various sphingolipids. The molar ratio of sphingolipid, PC, Chol, and *N*-NBD-PE in the liposome was 1.5:3:5:0.5. The liposomes were incubated with 10 μg/ml GST or GST-NT-Lys. The mixture was then subjected to a sucrose gradient centrifugation and fractionated from the top (*1–9*). The same volume from each fraction was subjected to SDS-PAGE and blotted against anti-GST antibody. Fluorescence intensity of *N*-NBD-PE was also measured to monitor the position of liposomes in the gradient. *Fr*, fraction. *E*, GST-NT-Lys does not form oligomers. The

TABLE I
Kinetic analysis of GST-NT-Lys binding to sphingomyelin

Kinetic analysis of GST-NT-Lys binding to immobilized phospholipid membranes was performed as described previously (12). SM/dipalmitoylphosphatidylcholine (8:2) liposome was immobilized to the hydrophobic alkanethiol sensor chip. Liposome consisting of dipalmitoylphosphatidylcholine alone was taken as a control. Various concentrations of GST-NT-Lys were injected over the immobilized lipid membrane surface. The binding kinetics were analyzed according to the manual of the software BIAevaluation 3.0.

	k_{on}	k_{off}	K_D
	$M^{-1}\ s^{-1}$	s^{-1}	M
GST-NT-Lys	6.2×10^4	1.2×10^{-2}	1.9×10^{-7}
Lysenin (from Ref. 12)	3.2×10^4	1.7×10^{-4}	5.3×10^{-9}

domain software. Obtained data were analyzed with Ripley's K-function using SPSS 2.0 software.

Intracellular Free Ca^{2+} Measurement—Jurkat cells were harvested from the growth medium, and 1×10^7 cells were resuspended in 1 ml of RPMI 1640 medium containing 0.5% bovine serum albumin. Fura-2AM (Dojin Kagaku) was added to the cells at the final concentration of 3 μM. After 30 min at 35 °C, the cells were washed twice with Fura-2 solution (0.1% bovine serum albumin, 25 mM Hepes (pH 7.0), 140 mM NaCl, 5 mM KCl, 1 mM $NaHPO_4$, 0.1% glucose, 0.5 mM $MgCl_2$, and 1 mM $CaCl_2$) and resuspended in 3 ml of the same solution. The ratio of the light intensity emitted at 505 nm upon dye excitation at the two wavelengths 340 and 380 nm at 35 °C was measured every other second using an FP-6500 spectrofluorometer equipped with a thermostatic cell holder (Jasco, Tokyo, Japan). When indicated as EGTA buffer, EGTA (pH 8.0) was added to the buffer at the final concentration of 1 mM. For SMase treatment, SMase (1.25 units/ml) was added during Fura-2AM loading.

Sphingomyelin Cross-linking and Western Blotting—3×10^6 Jurkat cells were washed with PBS twice, incubated with 50 μg/ml GST or GST-NT-Lys for 30 min at room temperature, and then incubated with or without 10 μg/ml monoclonal anti-GST antibody. Cells were suspended in RPMI 1640 medium and replated onto 12-well plates precoated with anti-mouse Ig antibody as described previously (26). After the indicated period, an equal volume of cell lysis buffer containing 10 mM Tris hydrochloride (pH 7.5), 10 mM EDTA, 150 mM NaCl, 2 mM Na_3VO_4, 20 mM NaF, and 2% Triton X-100 was added. Samples were subjected to SDS-PAGE and Western blotting as described previously (27).

Transfection—3–5 $\times$ 10^6 cells were suspended in Nucleofector™ solution V and then 3 μg of pIM21-H-Ras N17, which codes for a dominant negative form of H-Ras with mRFP under an internal ribosome entry site sequence, was introduced using program C-16 of the Nucleofector device (Amaxa). 72 h later, the cells were utilized for analysis.

RESULTS

Characterization of Deletion Mutants of Lysenin—In the previous study, we used native lysenin or full-length recombinant lysenin to characterize the organization of SM on plasma membranes (13, 15). One drawback of using full-length lysenin is its toxicity. Recently we examined the role of tryptophan residues of the protein on the recognition of SM and the cell toxicity (14). Systematic tryptophan to alanine mutation resulted in either the loss of both SM recognition and cell killing activities or no significant alteration of both activities. In the present study we prepared a series of deletion mutants of lysenin and measured their SM binding and hemolytic activities. Fig. 1*A* indicates the list of these deletion mutants. Mutants were tagged with MBP at their N termini and expressed in *E. coli*. The cytotoxicity of the MBP-conjugated mutants was analyzed by measuring hemolysis against sheep erythrocytes, whereas the recognition of SM was assessed by immunofluorescence labeling of fibroblasts from a NPA patient (14). NPA cells are deficient in acid SMase activity and therefore accumulate SM in late endosomes/lysosomes. As shown in Fig. 1*A*, deletion of C-terminal amino acids diminished the recognition of SM by lysenin. In contrast, lysenin could bind SM even after removal of N-terminal amino

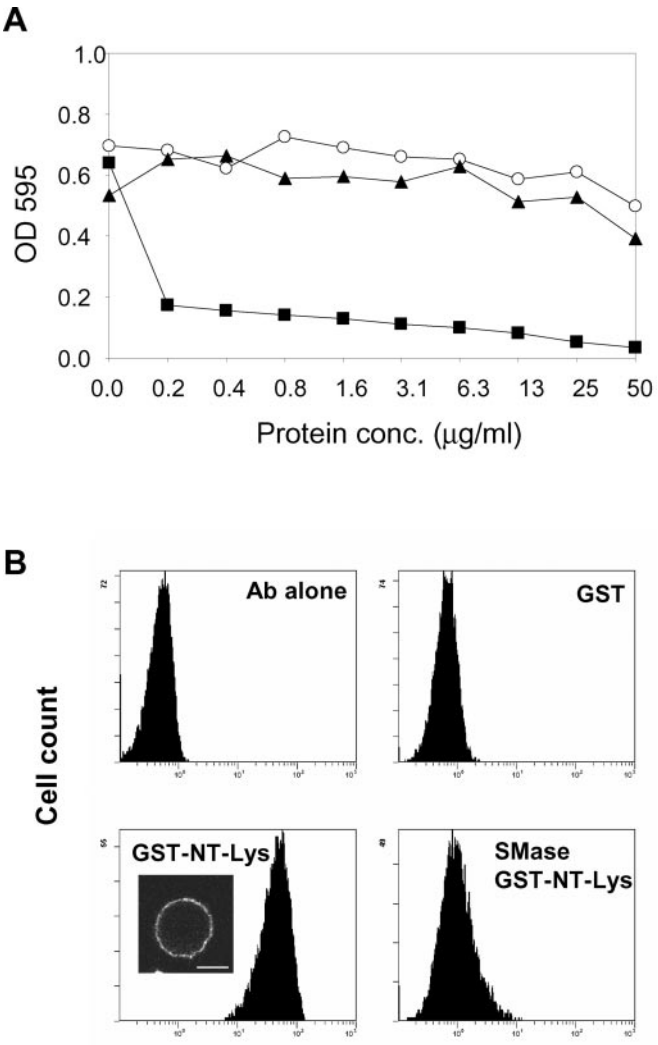

FIG. 2. **Recognition of SM by GST-NT-Lys in living cells.** *A*, MTT assay of Jurkat cells. 1×10^6 Jurkat cells were washed twice with PBS; incubated with various concentrations of GST (*open circles*), GST-NT-Lys (*closed triangles*), and GST-lysenin (*closed squares*) for 30 min at room temperature; resuspended in RPMI 1640 medium without sera, and cultured in the presence of 0.5 mg/ml MTT at 37 °C. After 4 h, MTT solution was removed, and cells were disrupted by the addition of Me_2SO. The absorbance at 595 nm was measured with a spectrophotometer. *B*, FACS analysis of Jurkat cells. 1×10^6 Jurkat cells were washed with PBS twice, incubated with 50 μg/ml GST or GST-NT-Lys for 30 min at room temperature, and incubated with or without 10 μg/ml monoclonal anti-GST antibody followed by goat anti-mouse IgG antibody conjugated with Alexa 488. For SMase treatment, cells were treated with SMase at 37 °C for 30 min prior to incubation with GST-NT-Lys. *Inset*, immunofluorescent image of a GST-NT-Lys-labeled cell. Jurkat cells were incubated with GST-NT-Lys, anti-GST, and Alexa 488-conjugated anti-mouse antibody as described above. Living cell images were obtained by confocal microscopy as described under "Materials and Methods." *Bar*, 10 μm.

liposomes composed of SM/Chol/*N*-NBD-PE (4:5:1) were incubated with 6.6 μg/ml GST-lysenin or 10 μg/ml GST-NT-Lys. The mixture was then subjected to sucrose gradient centrifugation and fractionated from the top (*1–9*). The same volume from each fraction was subjected to SDS-PAGE and blotted against anti-GST antibody. *O* and *M* indicate the oligomer and monomer form of GST-lysenin, respectively. *F*, immunofluorescence detection of the recognition of cellular SM by GST-NT-Lys. NPA fibroblasts were fixed, permeabilized, and incubated with GST alone or GST-NT-Lys followed by treatment with anti-GST and -CD63 antibodies and the corresponding secondary antibodies conjugated with Alexa 488 and 546, respectively. *Bar*, 20 μm.

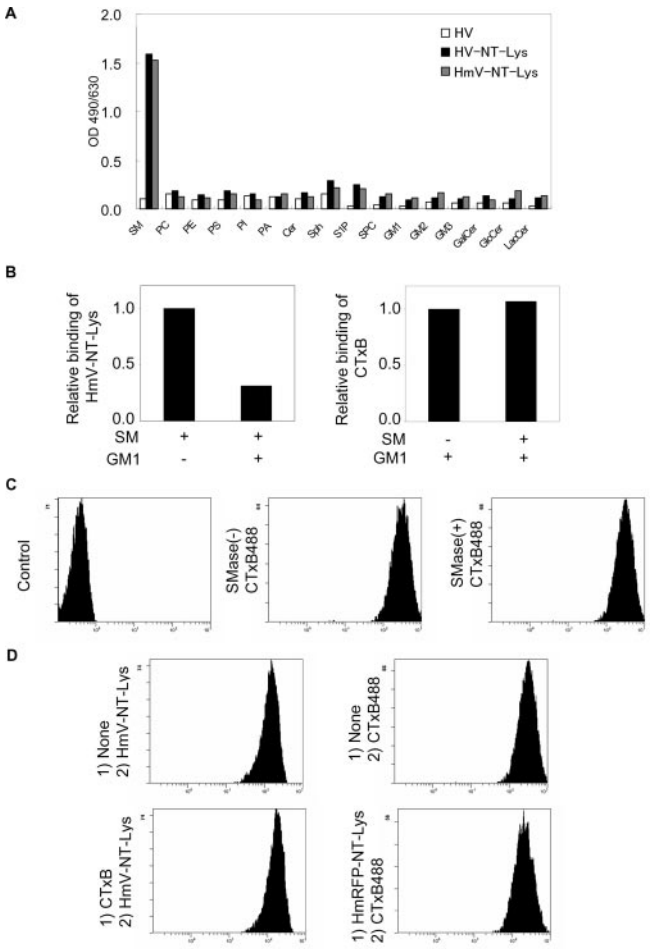

FIG. 3. **Recognition of SM and GM1 by lysenin and CTxB.** *A*, both HV-NT-Lys and HmV-NT-Lys specifically recognize SM. The binding to various lipids was examined by ELISA as described under "Materials and Methods." 25 μg/ml protein was used. *PE*, phosphatidylethanolamine; *PS*, phosphatidylserine; *PI*, phosphatidylinositol; *PA*, phosphatidic acid; *Cer*, ceramide; *Sph*, sphingosine; *SPC*, sphingosylphosphorylcholine; *GalCer*, galactosylceramide; *GlcCer*, glucosylceramide; *LacCer*, lactosylceramide; *GM3*, NeuAcα2,3Galβ1,4Glcβ1,1′-ceramide. *B*, the presence of GM1 inhibits the binding of HmV-NT-Lys to SM-containing liposomes. *Left*, liposomes composed of SM/PC/GM1/*N*-NBD-PE (1:4:0:0.25, *SM+ GM1−* or 1:4:1:0.5, *SM+ GM1+*) incubated with HmV-NT-Lys were fractionated by sucrose density gradient as described in the legend for Fig. 1*D*. The bound protein was quantitated by SDS-PAGE and Western blotting using anti-GFP antibody. *Right*, liposomes composed of SM/PC/GM1/*N*-NBD-PE (0:4:1:0.25, *SM− GM1+* or 1:4:1:0.5, *SM+ GM1+*) incubated with CTxB were fractionated and quantitated by dot blotting against anti-CTxB antibody. Representative results from two independent experiments are shown. *C*, SMase treatment does not affect CTxB binding to Jurkat cells. Cells were incubated with or without SMase for 30 min followed by incubation with Alexa 488-conjugated CTxB. The labeling of CTxB was monitored by FACS. *D*, pretreatment of Jurkat cells with one lipid probe does not affect the binding of the other. Cells were incubated with either CTxB or HmRFP-NT-Lys (denoted as "*1) CTxB*" or "*1) HmRFP-NT-Lys*") for 30 min on ice followed by 30-min treatment with HmV-NT-Lys or Alexa 488-conjugated CTxB on ice (denoted as "*2) HmV-NT-Lys*" or "*2) CTxB488*"). As a control, cells were incubated without any probe (denoted as "*1) None*"). The fluorescence was monitored by FACS as described in the legend for Fig. 2*B*.

acids. The minimal fragment that could recognize SM contained amino acids 161–297 of lysenin. Hereafter we refer to this minimal peptide as NT-Lys. It is noteworthy that all deletion mutants lost their hemolytic activity.

Changing the tag from MBP to GST did not alter the activity of the lysenin mutants. In Fig. 1, *B* and *C*, the binding specificity of GST-lysenin and the deletion mutant GST-NT-Lys was compared by ELISA. As shown in Fig. 1*B*, GST-NT-Lys had lower affinity than GST-lysenin. However, both GST-lysenin and GST-NT-Lys selectively bound SM. Slightly positive signals were obtained with sphingosine 1-phosphate (S1P) and sphingosylphosphorylcholine in both GST-lysenin and GST-NT-Lys. Other phospholipids, sphingolipids, or glycolipids bound neither GST-lysenin nor GST-NT-Lys. GST alone did not bind to any lipids. The kinetic parameters of GST-NT-Lys binding to SM were then determined using the BIAcore system, and the results were compared with those published for earthworm lysenin (12) (Table I). GST-NT-Lys and native lysenin showed comparable on-rate of binding to SM. In contrast, dissociation of GST-NT-Lys was 100 times faster than that of native lysenin. This is a 36-fold difference of overall K_D. To overcome this difference, we used relatively high concentrations of non-toxic lysenins compared with native lysenin throughout our experiments. In Fig. 1*D*, we examined the selective binding of GST-NT-Lys to SM using artificial membranes. Multilamellar liposomes composed of SM/PC/cholesterol (Chol), S1P/PC/Chol, or SPC/PC/Chol were prepared. All liposomes contained fluorescent phosphatidylethanolamine as a non-exchangeable liposome marker. After incubation with GST or GST-NT-Lys, liposomes were separated from unbound proteins by a flotation gradient. GST-NT-Lys floated up together with SM/PC/Chol liposomes, whereas GST alone remained at the bottom of the gradient. The GST-NT-Lys probe weakly bound to S1P/PC/Chol liposomes. GST-NT-Lys did not float up when SPC/PC/Chol liposomes were used. These results indicate that GST-NT-Lys selectively binds SM-containing membranes. Native and full-length lysenins oligomerize in the presence of sphingomyelin (13). The oligomerization is accompanied by pore formation in target membranes. Unlike native lysenin, SM did not induce oligomerization of GST-NT-Lys as shown in Fig. 1*E*. The recognition of cellular SM by GST-NT-Lys was then examined by measuring the binding of GST-NT-Lys to fixed and permeabilized NPA fibroblasts. Like native and non-truncated lysenin, GST-NT-Lys labeled intracellular organelles that are co-localized with tetraspanin CD63, which is enriched in lysosomes/late endosomes (28–30) (Fig. 1*F*). GST alone did not stain the cells.

In Fig. 2*A*, the toxicity of mutant lysenin against Jurkat cells was examined using MTT assay. Although GST-conjugated wild type lysenin showed toxicity at as low as 0.2 μg/ml, GST-NT-Lys did not significantly affect the viability of cells up to 50 μg/ml. This result, together with the result of Fig. 1, indicates that GST-NT-Lys is not toxic to nucleated cells or to red blood cells. Low toxicity of NT-Lys mutant made it possible to specifically label cell surface SM of living cells. In Fig. 2*B*, living Jurkat cells were labeled with GST-NT-Lys followed by incubation with anti-GST antibody and the corresponding Alexa 488-conjugated secondary antibody. FACS analysis indicated a significant increase of fluorescence intensity under these conditions (Fig. 2*B*, *GST-NT-Lys*). In contrast, cells were not significantly labeled when anti-GST alone and fluorescence-conjugated secondary antibodies were added (Fig. 2*B*, *Ab alone*) or when GST was used instead of GST-NT-Lys (Fig. 2*B*, *GST*). Fluorescence was also abolished when cells were pretreated with bacterial SMase. These results indicate that GST-NT-Lys recognizes cell surface SM in living Jurkat cells.

Mutant Lysenin Reveals the Spatial Heterogeneity of Cell Surface Lipid Raft Components—CTxB is a well known lipid marker for lipid rafts (31, 32). Using two lipid-specific toxins, lysenin and CTxB, we examined the detailed distribution of lipid components of lipid rafts. To examine the distribution of cell surface SM, we prepared fluorescent lysenin mutants. For this purpose, we used a recently developed GFP-derived fluorescent protein, Venus (19). Although GFP and related proteins

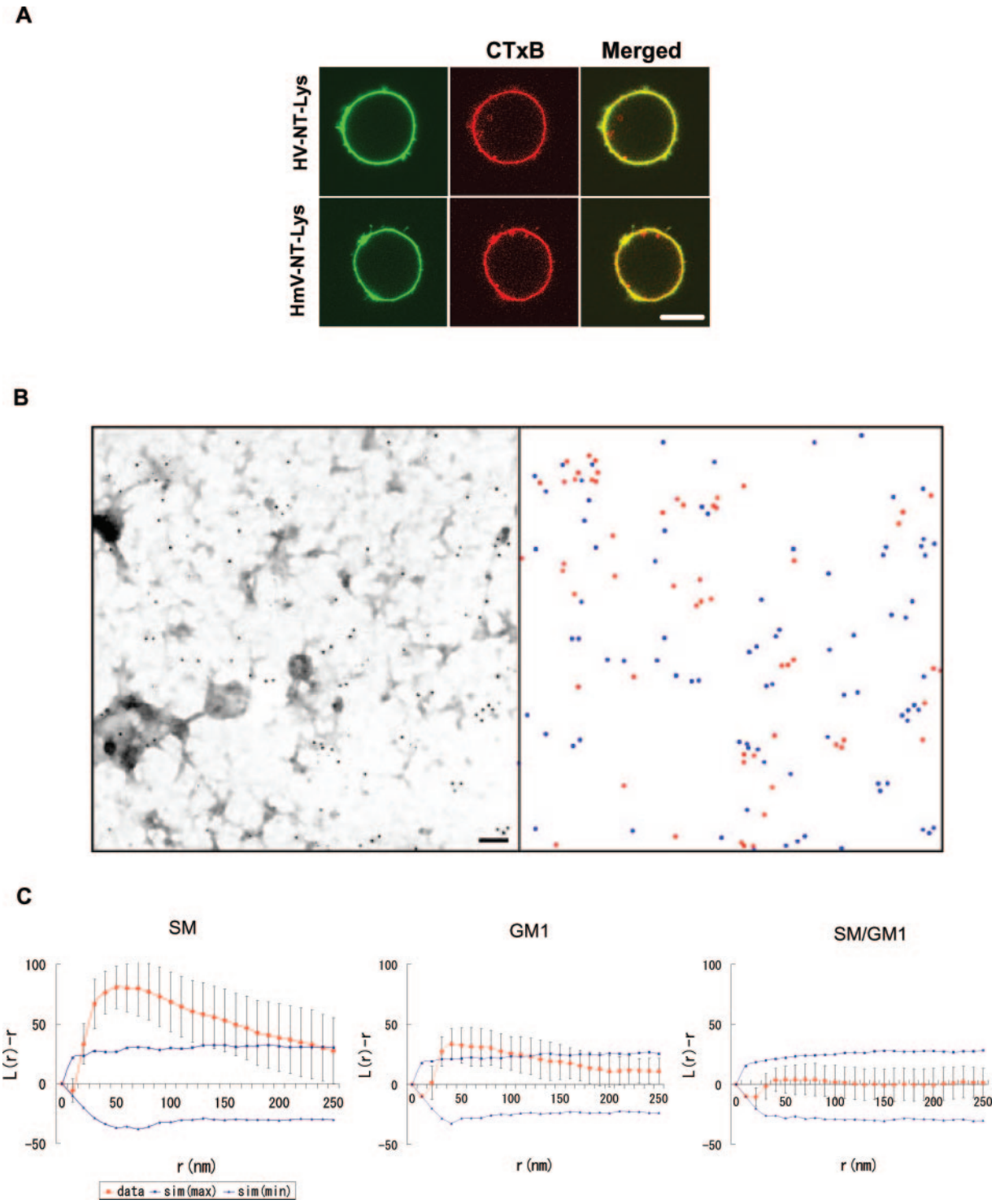

FIG. 4. **Cell surface distribution of SM-rich domains and GM1-rich domains.** *A*, immunofluorescent images of Venus-tagged NT-Lys. Jurkat cells were incubated with HV-NT-Lys or HmV-NT-Lys in the presence of CTxB-conjugated with Alexa 594. Living cell images were obtained by confocal microscopy as described under "Materials and Methods." *Bar*, 10 μm. *B*, distribution of SM-rich domains and GM1-rich domains on two-dimensional sheets of plasma membrane. Jurkat cells were first labeled with HmV-NT-Lys and biotinylated cholera toxin B fragments at 4 °C and then fixed with 4% paraformaldehyde and 0.02% glutaraldehyde for 10 min at 4 °C. The fixed cells were labeled with anti-GFP rabbit polyclonal antibody at 4 °C followed by labeling with goat anti-rabbit IgG-5-nm gold and goat anti-biotin IgG-10-nm gold at 4 °C. The distribution of gold particles on the plasma membrane was examined under electron microscope after ripping off as described under "Materials and Methods." *Bar*, 100 nm. In the *right panel*, distribution of SM (5-nm gold) is colored in *red*, whereas the distribution of GM1 (10-nm gold) is in *blue*. *C*, analysis of the distribution of SM-rich domains and GM1-rich domains using Ripley's K-function. EM images were analyzed as described under "Materials and Methods." Both SM-rich domains and GM1-rich domains form clusters, whereas the pairwise values for SM and GM1 fall within *blue lines* that represent the range of values expected for pairs of different particles whose distribution are random.

have a tendency to form oligomers, introduction of a single alanine to lysine substitution (A206K) prevents oligomerization (20). cDNA of His-tagged Venus or Venus A206K were fused to the 5′ terminus of NT-Lys. The chimeric proteins were expressed in *E. coli* and purified. The resulting HV-NT-Lys and HmV-NT-Lys were examined for their ability to bind SM in ELISA (Fig. 3*A*). Like MBP-NT-Lys and GST-NT-Lys, both fluorescent lysenin mutants specifically bound SM. Using

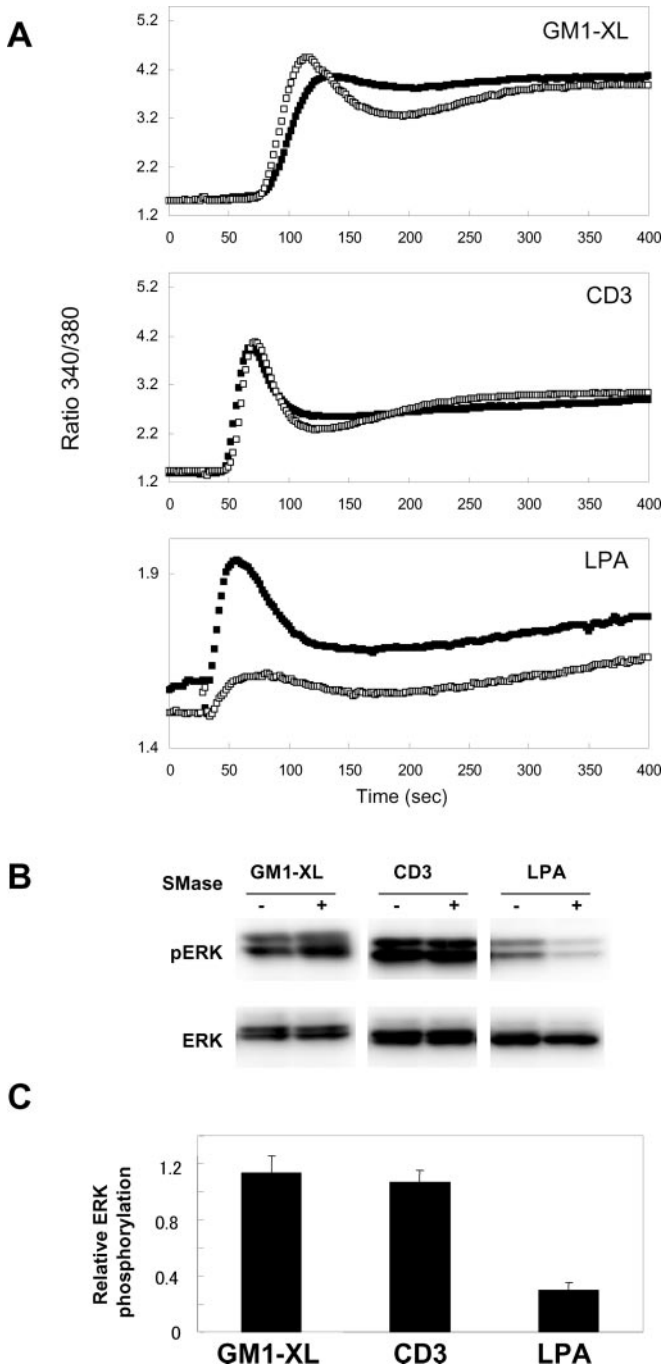

FIG. 5. **SMase treatment reveals existence of SM-related and non-related signal pathways.** *A*, cells were pretreated with (*open squares*) or without (*closed squares*) SMase in the presence of Fura-2AM indicator for 30 min at 35 °C. Cells were washed with calcium-containing buffer and stimulated with 1 μg/ml anti-CD3 antibody or 20 μM LPA for 10 min. For GM1 cross-linking (*GM1-XL*), cells were labeled with CTxB followed by incubation with anti-CTxB antibody for 15 min. Intracellular calcium was measured as described under "Materials and Methods." *B*, cells were pretreated with or without SMase and stimulated with the indicated reagents. The phosphorylated ERK (*pERK*) was visualized with a phosphospecific antibody. In *C*, relative ERK activation was calculated as (phospho-ERK with SMase treatment)/(phospho-ERK without SMase treatment).

mRFP (23), HmRFP-NT-Lys was also prepared, and its specific binding to SM was confirmed (data not shown).

Recently we have shown that lysenin recognizes SM in a local density-dependent manner. Model membrane experiments indicated that glycolipids altered the local density of SM so that the affinity of lysenin for the lipid was decreased (15). The observed effect was not due to steric hindrance because other gel-phase lipids such as dipalmitoylphosphatidylcholine showed a similar effect. Fig. 3*B* shows that the presence of GM1 in SM-containing liposomes hindered the binding of HmV-NT-Lys. A similar effect was observed with GM2, which has a smaller head group than GM1 (data not shown). In contrast, the binding of CTxB to ganglioside GM1 was not affected by the presence of SM. This observation was further supported with the finding that SMase treatment did not affect binding of Alexa 488-conjugated CTxB to living Jurkat cells (Fig. 3*C*). The prior binding of cholera toxin did not affect the binding of HmV-NT-Lys (Fig. 3*D*). Similarly pretreatment of Jurkat cells with lysenin mutant did not alter the binding of CTxB. These results, together with our previous observation, indicate that, whereas lysenin recognizes a specific subset or specific distribution of sphingomyelin molecules, CTxB recognizes GM1 irrespective of the distribution of the lipids. Because pretreatment of one toxin did not affect the binding of the other, either they do not compete for binding or the lipids are spatially segregated.

Our results indicate that, although non-toxic, NT-Lys keeps the characteristics of earthworm lysenin and efficiently labels cell surface SM-rich membrane domains if the appropriate concentration is used. When plasma membranes of living Jurkat cells were doubly labeled either with HV-NT-Lys and CTxB or with monomeric HmV-NT-Lys and CTxB, cells were evenly stained with both green and red fluorescence (Fig. 4*A*), supporting the idea that the size of the lipid domains are below the resolution of the fluorescence microscope. The distribution of GM1 and SM was further examined on fixed two-dimensional sheets of plasma membrane ripped off from cells directly onto EM grids (24, 25, 33–35) (Fig. 4*B*). Membrane fragments trapped on the EM grids are composed largely of flat areas of cell membranes. They are easily distinguished from contaminating structures containing ER or Golgi membrane or cytoskeleton under the electron microscope. We selected the flat area without contamination for the present image analysis (25, 35). Cells were doubly labeled with HmV-NT-Lys and biotinylated CTxB at low temperature followed by fixation with paraformaldehyde and glutaraldehyde. Cells were further incubated with anti-GFP antibody and anti-rabbit IgG (5-nm gold) to visualize SM-rich membranes and anti-biotin IgG (10-nm gold) to mark GM1. Both SM and GM1 were distributed over the whole membrane. The gold patterns were further analyzed by using Ripley's K-function (24, 25). Ripley's K-function evaluates all interparticle distances over the study area and compares the observed distribution of gold particles with that expected from complete spatial randomness. This analysis focuses the second-order properties of gold distribution and has the advantage that it analyzes spatial structure at multiple ranges simultaneously. The *solid horizontal line* at 0 in Fig. 4*C* gives the expected value for $L(r) - r$ under complete spatial randomness. The *blue lines* (sim(max) and sim(min)) give a 99% confidence envelope for complete spatial randomness from 100 simulations. In Fig. 4*C*, the experimental values for $L(r) - r$ (*red lines*) are plotted relative to reference values (*blue lines*). K-function analysis of SM distribution showed that the gold pattern is clustered, *i.e.* the curve showed significant positive deviation from the *blue lines*. The maximum deviation occurred at a radius of 60–80 nm, indicating that SM forms domains with a radius of 60–80 nm. GM1 also formed domains with a similar radius. In contrast, the pairwise values for SM and GM1 fell within the *blue lines* (Fig. 4*C*, *SM/GM1*), indicating that colocalization of SM-rich domains and GM1-rich domains is not significant. Our results indicate that plasma membrane SM-rich domains are spatially distinct from ganglioside GM1-rich membrane domains.

Sphingomyelinase Treatment Reveals the Existence of SM-related and Non-related Signal Pathways—It is well established that, upon binding of antigen to lymphocyte receptors, the calcium release from intracellular stores is up-regulated followed by the induction of influx via calcium channels on the plasma membrane (36, 37). Cross-linking of T cell receptor (TCR)-CD3 complex with anti-CD3 antibody mimics the presentation of antigen. Similarly the binding of CTxB to Jurkat cells induces both the release of Ca^{2+} from the intracellular stores and a Ca^{2+} influx from extracellular spaces (38). Binding of the CTxB pentamer induces the clustering of five GM1 molecules (39). Antibody against CTxB enhances this clustering (40). Our results indicate that SM-rich domains are spatially distinct from GM1-rich domains on the plasma membranes of Jurkat cells. We asked whether SM-rich domains are functionally related to GM1-rich domains. To examine this possibility, Jurkat cells were treated with *B. cereus* SMase to deplete cell surface SM followed by various stimulations. As shown in Fig. 5*A*, SMase treatment did not significantly affect the Ca^{2+} increase induced by anti-CD3 antibody or by cross-linking of GM1. LPA is reported to increase intracellular calcium and ERK activation through its receptor, LPA1/2/3, a member of the G-protein-coupled receptor family, followed by activation of phospholipase C (PLC) β via the G-protein G_q (41). In contrast to CD3 and GM1 stimulation, the LPA-induced calcium increase was dramatically decreased by SMase treatment.

ERK1/2 are key regulators of cytokine production in T cells (42). Both ERK1 (p44 mitogen-activated protein kinase) and ERK2 (p42 mitogen-activated protein kinase) belong to a family of protein serine/threonine tyrosine kinases that are activated by a variety of growth factors as well as by other extracellular stimuli. Activation of ERK1/2 occurs through phosphorylation of threonine and tyrosine (202 and 204) by a MAPK kinase (MAPKK or MEK), which is activated by a MAPKK or MEK kinase (MAPKKK or Raf family). Anti-CD3 antibody, CTxB, and LPA treatment of Jurkat cells induces ERK phosphorylation. Fig. 5, *B* and *C*, shows that SMase treatment selectively inhibited LPA-mediated ERK phosphorylation. Our results indicate that SM is important for signaling through LPA. In contrast, SM was dispensable for the signal transduction initiated by cross-linking of TCR or GM1.

Cross-linking of SM-rich Domain Provides a Signaling Platform That Is Distinct from Those Induced by Cross-linking of TCR or GM1—We then asked whether cross-linking of SM-rich membrane domains provides a signaling platform as observed in cross-linking of TCR or GM1. In Fig. 6*A*, Jurkat cells were loaded with the calcium indicator Fura-2AM, and intracellular Ca^{2+} was monitored both in the presence and the absence of Ca^{2+} in the media. Stimulation of TCR-CD3 by a specific antibody increased intracellular Ca^{2+} both in the presence and absence of extracellular Ca^{2+} under these conditions (Fig. 6*A*, *upper left*). Addition of GST-NT-Lys did not significantly affect intracellular Ca^{2+}. GST had no effect (Fig. 6*A*, *upper right*). Next cells were labeled with GST-NT-Lys on ice, loaded with Fura-2AM at 35 °C, and stimulated with anti-GST antibody (Fig. 6*A*, *lower left*). A sustained increase of Ca^{2+} was observed in the presence of exogenous Ca^{2+}. However, unlike CD3 stimulation, Ca^{2+} release was not significantly observed in the absence of extracellular Ca^{2+}. We then labeled cells with GST-NT-Lys and anti-GST antibody on ice, loaded with Fura-2AM at 35 °C, and stimulated with the corresponding secondary antibody. Cross-linking was further enhanced by the addition of a secondary antibody (Fig. 6*A*, *lower right*). Under these conditions, intracellular calcium was increased both in the absence and the presence of EGTA. Anti-CD3-induced calcium influx from the extracellular space was inhibited by nifedipine, a blocker of the L-type Ca^{2+} channel, to an extent similar to calcium chelation (Fig. 6*B*, *left*). In case of GST-NT-Lys and anti-GST antibody-induced calcium influx, treatment with Me_2SO, a solvent of nifedipine, slightly inhibited calcium influx. However, the addition of nifedipine significantly blocked calcium influx (Fig. 6*B*, *right*). In Fig. 6*C*, phosphorylation of ERK was examined after cross-linking of SM-rich domains. In this experiment, Jurkat cells incubated with GST-NT-Lys were replated onto plates coated with anti-GST antibody (*left panel*). Alternatively cells were incubated with GST-NT-Lys and anti-GST antibody followed by replating onto plates coated with the corresponding secondary antibody (*right panel*). Under this condition, cells attached to the plates slowly, thus giving a low ERK signal after a 3-min incubation because of detachment of the cells. Phosphorylation of ERK was observed in both cases in the presence of GST-NT-Lys. Our results thus indicate that the cross-linking of SM-rich domain provides a calcium signaling and ERK activation platform.

Upon anti-CD3 antibody stimulation, ERK1/2 phosphorylation is induced via tyrosine kinase cascade (43). It has also been reported that the cross-linking of GM1 with CTxB and its corresponding antibody induces local accumulation of protein tyrosine phosphorylation (40). We asked whether tyrosine phosphorylation was involved in signal transduction mediated by the cross-linking of SM. Although anti-CD3 antibody induced tyrosine phosphorylation, cross-linking of SM by GST-NT-Lys did not significantly affect phosphorylation (Fig. 7*A*). Both anti-CD3 antibody and GST-NT-Lys activated ERK to a similar extent (Fig. 7*C*, *fourth* and *fifth rows*). As previously described, GM1 cross-linking with CTxB and anti-CTxB antibody induced a pattern of tyrosine phosphorylation similar to that induced by anti-CD3 antibody stimulation (Fig. 7*B*).

LAT is an adaptor protein that performs a critical function in TCR-mediated signal transduction (44). LAT is reported to be tyrosine phosphorylated by ZAP-70 upon TCR/CD3 stimulation or CTxB engagement to GM1 in T cells (38). LAT was immunoprecipitated from the cell lysates after treatment of Jurkat cells with anti-CD3 antibody or with GST-NT-Lys. The samples were blotted against phosphorylated tyrosine-specific antibody after SDS gel electrophoresis (Fig. 7*C*, *second row*). Whereas anti-CD3 antibody treatment induced tyrosine phosphorylation of LAT, only a slight up-regulation of phosphorylation of LAT was observed after GST-NT-Lys treatment (Fig. 7*C*, *second row*). This observation was confirmed by using anti-phosphotyrosine antibody for amino acid 191 of LAT protein (Fig. 7*C*, *first row*). These results indicate that, unlike CD3 or GM1, cross-linking of SM-rich domains very weakly induces protein tyrosine phosphorylation.

Signaling Molecules Related to Lck Are Necessary for ERK Activation by Cross-linking SM-rich Domains—Lck is the key regulator for TCR-mediated signaling events. Tyrosine phosphorylation of ZAP-70 and PLCγ1 by activated Lck up-regulates their activities (43, 45). Chemical mutagenesis generated mutant Jurkat cell lines, JCaM1.6 (46), J.gamma1 (47), P116 (48), and J45.01 (49), that are defective in Lck, PLCγ, ZAP-70, and CD45 expression, respectively. We examined phosphorylation of ERK in these cell lines after different stimulation. As shown in Fig. 8*A*, ERK phosphorylation induced by cross-linking of SM-rich domains was severely blocked in Lck-, ZAP-70-, and CD45-defective mutants, and approximately 40% inhibition was observed in PLCγ1-defective mutants. CD45 is a transmembrane tyrosine phosphatase that positively regulates Lck activity (49), and ZAP-70 is a protein kinase located downstream of Lck (48). These results indicate that the CD45-Lck-ZAP-70 cascade is necessary for ERK phosphorylation by SM

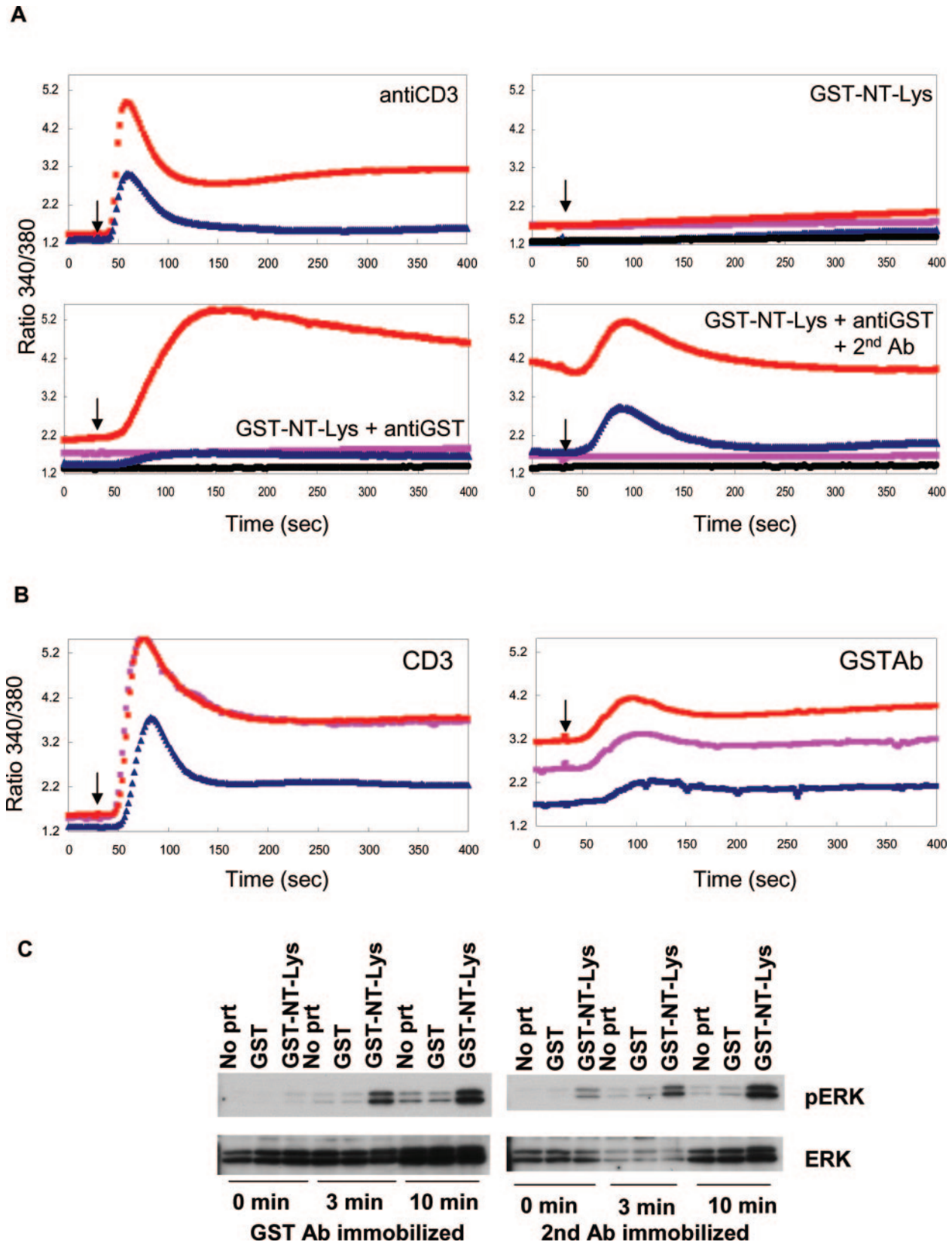

FIG. 6. **Induction of calcium influx and ERK activation by cross-linking of SM-rich domains.** *A*, cross-linking of SM-rich domains induces calcium influx. Jurkat cells were loaded with Fura-2AM as described under "Materials and Methods," and the proteins were added at 30 s (indicated by *arrows*). *Upper left*, *red squares* show the result in the presence of 1 mM calcium buffer, and *blue triangles* show the result in the presence of 1 mM EGTA. 1 μg/ml anti-CD3 antibody was added. In the remaining panels, *red squares* and *blue triangles* are the results from cells incubated with GST-NT-Lys and measured in the presence of calcium or EGTA, respectively. *Pink squares* and *black circles* are the results from cells incubated with GST and measured in the presence of calcium or EGTA, respectively. *Upper right*, GST or GST-NT-Lys was added at 30 s after loading Fura-2AM. *Lower left*, cells were first labeled with GST or GST-NT-Lys on ice for 30 min and then loaded with Fura-2AM, and anti-GST antibody was added as indicated by the *arrow*. *Lower right*, cells were labeled with proteins and anti-GST antibody on ice and loaded with Fura-2AM, and anti-mouse Ig antibody was added as indicated by the *arrow*. Results shown here are representative data from at least two

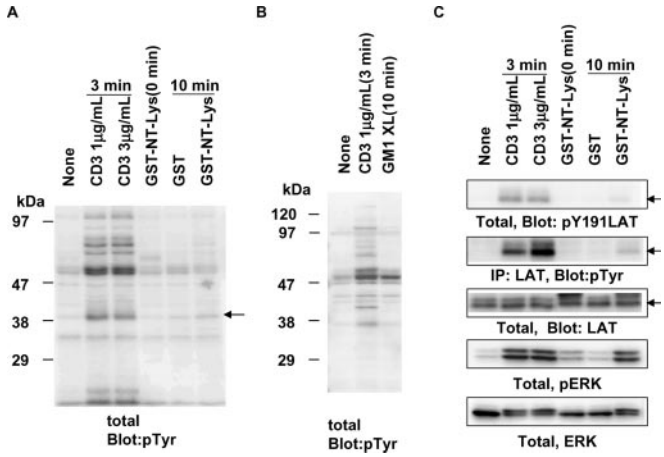

FIG. 7. **Cross-linking of SM-rich domains only slightly induces protein tyrosine phosphorylation.** *A*, Jurkat cells were stimulated for 10 min according to the protocol described in the legend of Fig. 6*A*, *lower left panel*. Cell lysates were separated by SDS-PAGE and blotted against anti-phosphotyrosine antibody as described under "Materials and Methods." As a positive control, cells were stimulated with anti-CD3 antibody without cross-linking for 3 min. An *arrow* indicates the band corresponding to LAT designated by the molecular mass. *B*, Jurkat cells were labeled with CTxB on ice for 30 min followed by the cross-linking (*XL*) with anti-CTxB antibody at 37 °C for 10 min. As a control, cells were stimulated with anti-CD3 antibody as described above. *C*, cells were stimulated as described in *A*. Cell lysates were separated by SDS-PAGE and blotted as indicated. To immunoprecipitate (*IP*) LAT protein, cell lysates were incubated with anti-LAT antibody followed by incubation with agarose beads conjugated with protein A. Immunoprecipitates were separated by SDS-PAGE and blotted against anti-phosphotyrosine antibody. *Arrows* indicates bands corresponding to LAT protein. *pTyr*, phosphotyrosine; *pERK*, phospho-ERK.

aggregation. Although PLCγ1 is positively regulated by tyrosine phosphorylation by Lck (45), its role for ERK activation by SM cross-linking was limited. LPA-induced ERK phosphorylation was partially inhibited in the mutants, whereas Lck was required for anti-CD3-dependent ERK phosphorylation.

PKC Is Required for SM Cross-linking-induced ERK Activation—The mechanism of phosphorylation of ERK by cross-linking of SM was further examined. It is well established that intracellular calcium levels regulate the activity of classical and novel types of PKC and that long term treatment with PMA decreases their expression (50). To examine the role of PKC upon ERK activation, Jurkat cells were treated with PMA for 48 h followed by cross-linking of SM. As shown in Fig. 8*B*, PMA treatment prevented the expression of PKCθ. In these cells, ERK activation by SM cross-linking was severely inhibited. We confirmed the expression of α, β, δ, and θ types of PKC in Jurkat cells and depletion of their expression by PMA treatment (data not shown).

In Fig. 8*C*, we examined the effect of various inhibitors on ERK phosphorylation mediated by cross-linking SM-rich domains. The degree of phosphorylation 10 min after GST-NT-Lys cross-linking was taken as one (Fig. 8*C*, *sixth bar* from the *left*). PD98059, an inhibitor for MEK (51), significantly reduced ERK activation. The result from cells depleted of PKC by PMA was also quantified. H89 is known as an inhibitor of cAMP-dependent protein kinase at low (50 nM) and several kinases including calmodulin kinase II, casein kinase, myosin light chain kinase, and PKC at high (10 μM) concentration (52). Treatment with H89 at high concentration severely inhibited ERK phosphorylation, whereas partial inhibition was observed at low concentration. PLC inhibitor U73122 (53), which acts both on β and γ types of PLC, inhibited phosphorylation down to the level of that in non-treated cells. These results suggest the involvement of a PLC-PKC and/or calmodulin-modulated calmodulin kinase II pathways in SM cross-linking-dependent signal transduction. The G$\alpha_{i/o}$-specific inhibitor pertussis toxin also inhibited ERK phosphorylation. Ras has been implicated in a Lck-ZAP-70-LAT-PLCγ1 cascade (54). Expression of a FLAG-tagged dominant negative form of H-Ras, which is expressed at levels 2–5-fold greater than endogenous Ras (data not shown), did not suppress ERK phosphorylation.

DISCUSSION

Using a non-toxic SM-rich domain-specific probe, we examined the distribution and function of SM-rich membrane domains in living cells. Our results indicate that SM-rich membrane domains are spatially and functionally different from those enriched with glycolipid GM1. Our results thus indicate the spatial and functional heterogeneity of lipid rafts.

Non-toxic Lysenin, a Unique Probe to Monitor Sphingomyelin-rich Membrane Domains in Living Cells—Lysenin is an SM-specific toxin isolated from the coelomic fluid of the earthworm *Eisenia foetida*. Lysenin comprises a family of proteins together with lysenin-related proteins 1 and 2 (14, 16, 55). Recently we have shown that lysenin recognizes SM in a distribution-dependent manner (15). Thus, this toxin binds SM only when SM forms aggregates or domains. Therefore, lysenin is a probe for SM-rich membrane domains. Upon binding to SM, lysenin assembles into SDS-resistant oligomers, leading to the formation of pores with a hydrodynamic diameter of ~3 nm (13). This toxicity of lysenin hindered the characterization of SM-rich domains in living cells. In the present study, we prepared a series of deletion mutants of lysenin. Our results indicate that the N terminus of this protein is not required for recognition of SM but is required for cytotoxicity. The presence of SM did not induce oligomerization of GST-NT-Lys, suggesting the requirement of the toxin oligomers for the cytotoxicity of lysenin. Lysenin contains six tryptophan residues of which five are conserved in lysenin-related proteins 1 and 2 (14). Our recent data suggest the importance of the conserved tryptophan residues for the toxic functions. Two conserved tryptophans reside in the N terminus of lysenin. Because these tryptophans are not required for the binding of SM, they are not directly involved in the recognition of SM. Deletion of the N terminus of lysenin did not affect the on-rate of the protein binding to SM. In contrast, dissociation of the protein was accelerated in the mutant lysenin. Because GST-NT-Lys did not oligomerize, this result suggests that oligomerization of lysenin stabilizes the binding of the protein to SM-containing membranes. Our results using model membranes indicate that, although non-toxic, NT-Lys keeps the characteristics of earthworm lysenin and efficiently labels

experiments. *B*, calcium channel blocker inhibits calcium influx triggered by cross-linking of SM-rich domains. *Left*, Jurkat cells were loaded with Fura-2AM in the absence of Me_2SO (*red squares*), in the presence of Me_2SO (*pink squares*), and in the presence of 200 μM nifedipine in Me_2SO (*blue triangles*). 1 μg/ml anti-CD3 antibody was added at 30 s as indicated by the *arrow*. *Right*, cells were incubated with GST-NT-Lys on ice for 30 min in the absence of Me_2SO (*red squares*), in the presence of Me_2SO (*pink squares*), and in the presence of 200 μM nifedipine in Me_2SO (*blue triangles*). Cells were then loaded with Fura-2AM and activated according to the protocol in *A*, *lower left*. Results shown here are representative data from at least two experiments. *C*, cross-linking of SM-rich domain induces ERK phosphorylation. Jurkat cells were incubated with 50 μg/ml GST or GST-NT-Lys or without any addition (*No prt*) and replated onto plates coated with anti-GST antibody (*left panel*), or cells were further incubated with anti-GST antibody and replated onto plates coated with the corresponding secondary antibody (*right panel*). After the indicated periods, cells were lysed and subjected to SDS-PAGE and Western blotting. *Upper row*, blotted against anti-phosphospecific antibody; *lower row*, anti-ERK antibody. *Ab*, antibody; *pERK*, phospho-ERK.

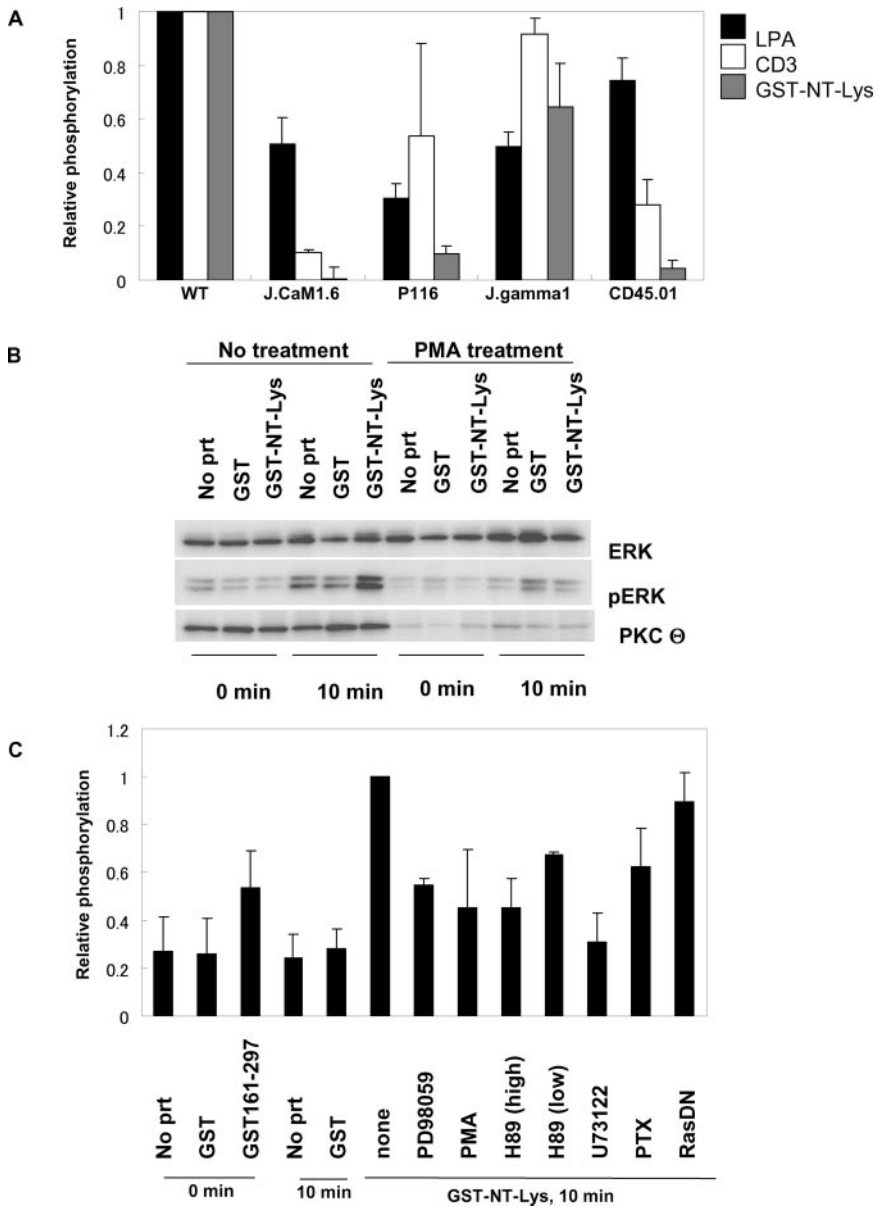

FIG. 8. **Effect of inhibitors on ERK activation induced by cross-linking of SM-rich domains.** *A*, mutants of Jurkat cells were stimulated as described in the legend for Fig. 6*C*, *right panel*. Intensity of phosphorylated ERK was measured using the LAS system (Fujifilm) and analyzed by Image Gauge (Fujifilm). The relative activation of ERK was calculated as (stimulation of ERK phosphorylation in mutant)/(stimulation of ERK phosphorylation in wild type). *B*, Jurkat cells were pretreated with 200 nM PMA for 48 h, stimulated, and analyzed as described in the legend of Fig. 6*C*, *right panel*. *No prt*, no protein pretreatment. *C*, Jurkat cells were treated in the presence or the absence of various inhibitors in the medium for 60 min at 37 °C. Concentrations of inhibitors were as follows: PD98059, 20 μM; U73122, 10 μM; H89 high, 10 μM; H89 low, 50 nM; and pertussis toxin (*PTX*), 100 ng/ml for 16 h. To express a dominant negative form of H-Ras (*RasDN*), a plasmid was introduced using an Amaxa transfection apparatus and cultured for 72 h. In parallel experiments, a plasmid coding GFP or yellow fluorescent protein (YFP) was introduced to monitor the transfection. Transfection efficiency was around 75–90%. Expression of the dominant negative form of H-Ras was also confirmed by Western blotting with anti-Ras antibody (data not shown). Cells were labeled with GST-NT-Lys followed by incubation with anti-GST antibody and stimulated for 10 min by plating onto a dish precoated with the secondary antibody. The relative activation of ERK was calculated as (phospho-ERK with inhibitor treatment)/(phospho-ERK without inhibitor treatment). Results are the average of three independent experiments. *WT*, wild type; *pERK*, phospho-ERK.

cell surface SM-rich membrane domains if the appropriate concentration is used.

Spatial Heterogeneity of the Lipid Rafts—Lipid rafts are defined as membrane microdomains enriched with sphingolipids and cholesterol. Micrometer scale heterogeneity of lipid raft components has been reported in migrating T cells and T cells after antigen stimulation (56, 57). These heterogeneities could be observed under a fluorescent microscope. However, the accumulating evidence suggests that, in steady state, the size of lipid rafts in biomembranes is much smaller (32, 58). Indeed, when living Jurkat cells were labeled with mutant lysenin or CTxB, fluorescence was evenly distributed along the cell surface (Fig. 4*A*). Biophysical methods detecting submicrometer scale interaction or specific probes that recognize lipid clusters are required to study small domains. Using fluorescence resonance transfer of fluorescently labeled CTxB, Kenworthy *et al.* (31) showed that clustering of GM1 does not occur on plasma membranes. Recently Glebov and Nichols (32) used the same procedure and found that at least part of the GM1 molecules exist as clusters. Using a combination of lysenin and SMase, we have shown that the organization of SM differs between different cell types and between different membrane domains within the same cell (15). Our results also support the idea of the existence of small condensed SM complexes consisting of just a few lipid molecules in living cells. Little is known about submicrometer scale heterogeneous organization of membrane lipids in biomembranes (59). Here we compared the distribution of SM-rich domains with that of GM1-rich domains. Our results indicate that the two lipid domains were distributed differently on the plasma membrane, indicating a spatial heterogeneity of SM-rich domains from GM1-rich membrane domains. It should be noted that GM1 inhibits the binding of lysenin to SM. Therefore "by definition" lysenin-labeled domains are devoid of GM1 at the molecular level. However, this does not exclude the possibility that the SM-rich domain and GM1-rich domain form mixed domains in the area of a radius of 60–80 nm. Our statistical analysis indicated the presence of submicrometer scale SM-rich domains and GM1-rich domains. However, our results revealed a lack of colocalization of SM-rich domains and GM1-rich domains. Because both SM and GM1 are well recognized as lipid raft markers, our results indicate heterogeneity of lipid rafts on a submicrometer scale.

Functional Heterogeneity of Lipid Rafts—The current view of raft domains is that they contain few raft molecules and ex-

change their components on a submillisecond scale (60). It is proposed that the cross-linking of raft components leads to a coalescence of rafts and that these stabilized raft domains function as signaling centers (7). Like T cell receptor activation and cross-linking of GM1, cross-linking of SM induces calcium influx and ERK phosphorylation in Jurkat cells. However, unlike CD3 or GM1, cross-linking of SM did not induce significant protein tyrosine phosphorylation. These results suggest that SM provides a functional signal cascade platform that is distinct from those provided by TCR or GM1. This idea was supported by our observation that SMase treatment of Jurkat cells abolished LPA-mediated but not TCR-dependent signal transduction. These results indicate that LPA-mediated signal transduction is functionally related to SM-rich membrane domains and is distinct from signal transduction pathways mediated by anti-CD3 antibody or cross-linking of GM1. LPA mediates signal transduction via its receptors, LPA1, -2, and -3, members of the so-called "endothelial differentiation gene (EDG)" family of G-protein-coupled receptors, and were previously called EDG2, -4, and -7, respectively (61). The $G\alpha_{i/o}$-specific inhibitor pertussis toxin inhibited ERK phosphorylation by cross-linking of SM-rich domains, suggesting that SM-rich domain-mediated signaling pathways pass through or locate downstream of G-protein-coupled receptor signaling.

Inhibitor experiments suggest the importance of intracellular calcium on ERK activation induced by the cross-linking of SM-rich domains. Calcium-regulated calcium/calmodulin-dependent protein kinase II (62) and PKC-Raf activation pathways (63–65) are reported to be utilized in ERK activation. A slight inhibition by expression of dominant negative H-Ras suggests that the tyrosine kinase-mediated Ras activation pathway is not the main pathway initiated by SM clustering. Although cross-linking of SM-rich domains did not induce significant protein tyrosine phosphorylation, studies using somatic mutants indicate the importance of the CD45-Lck-ZAP-70 tyrosine kinase cascade in NT-Lys-triggered ERK activation. One could speculate that a small amount of tyrosine phosphorylated proteins are sufficient to induce ERK phosphorylation by cross-linking SM-rich domains. Alternatively these molecules may work as scaffolding molecules as observed in the interaction with integrin (66). The involvement of tyrosine kinases in G-protein-coupled receptor pathway has been proposed. The $G\alpha_i$ and $G\alpha_s$ families of proteins can be tyrosine phosphorylated *in vitro* when they are immunoprecipitated by their antibodies (67). *In vivo* upon carbachol stimulation and overexpression of Fyn, $G\alpha_{q/11}$ proteins are tyrosine phosphorylated.

In conclusion, our results indicate that sphingomyelin-rich domains are spatially distinct from ganglioside GM1-rich membrane domains. Our results also suggest that the sphingomyelin-rich domain provides a functional signal cascade platform that is distinct from those provided by TCR or GM1. Our study therefore elucidates the spatial and functional heterogeneity of lipid rafts.

Acknowledgments—We thank the members of the Kobayashi laboratory and Dr. Kyoko Nakamura for support, critical reading of the manuscript, and discussion and Dr. Toshiyuki Yamaji for help in calcium measurements. We are grateful to Drs. Hitoshi Sakuraba, Takeharu Nagai, Atsushi Miyawaki, Michiyuki Matsuda, and Naoki Mochizuki for providing cells and plasmids and discussion.

REFERENCES

1. Dowhan, W. (1997) *Annu. Rev. Biochem.* **66,** 199–232
2. Balasubramanian, K., and Schroit, A. J. (2003) *Annu. Rev. Physiol.* **65,** 701–734
3. Zachowski, A. (1993) *Biochem. J.* **294,** 1–14
4. van Meer, G., and Simons, K. (1982) *EMBO J.* **1,** 847–852
5. Kobayashi, T., Storrie, B., Simons, K., and Dotti, C. G. (1992) *Nature* **359,** 647–650
6. Nakada, C., Ritchie, K., Oba, Y., Nakamura, M., Hotta, Y., Iino, R., Kasai, R. S., Yamaguchi, K., Fujiwara, T., and Kusumi, A. (2003) *Nat. Cell Biol.* **5,** 626–632
7. Simons, K., and Toomre, D. (2000) *Nat. Rev. Mol. Cell Biol.* **1,** 31–39
8. Edidin, M. (2003) *Annu. Rev. Biophys. Biomol. Struct.* **32,** 257–283
9. Simons, K., and Ikonen, E. (1997) *Nature* **387,** 569–572
10. London, E., and Brown, D. A. (2000) *Biochim. Biophys. Acta* **1508,** 182–195
11. Heerklotz, H. (2002) *Biophys. J.* **83,** 2693–2701
12. Yamaji, A., Sekizawa, Y., Emoto, K., Sakuraba, H., Inoue, K., Kobayashi, H., and Umeda, M. (1998) *J. Biol. Chem.* **273,** 5300–5306
13. Yamaji-Hasegawa, A., Makino, A., Baba, T., Senoh, Y., Kimura-Suda, H., Sato, S. B., Terada, N., Ohno, S., Kiyokawa, E., Umeda, M., and Kobayashi, T. (2003) *J. Biol. Chem.* **278,** 22762–22770
14. Kiyokawa, E., Makino, A., Ishii, K., Otsuka, N., Yamaji-Hasegawa, A., and Kobayashi, T. (2004) *Biochemistry* **43,** 9766–9773
15. Ishitsuka, R., Yamaji-Hasegawa, A., Makino, A., Hirabayashi, Y., and Kobayashi, T. (2004) *Biophys. J.* **86,** 296–307
16. Ishitsuka, R., and Kobayashi, T. (2004) *Anat. Sci. Int.* **79,** 184–190
17. Hasegawa, H., Kiyokawa, E., Tanaka, S., Nagashima, K., Gotoh, N., Shibuya, M., Kurata, T., and Matsuda, M. (1996) *Mol. Cell. Biol.* **16,** 1770–1776
18. Sekizawa, Y., Kubo, T., Kobayashi, H., Nakajima, T., and Natori, S. (1997) *Gene* (*Amst.*) **191,** 97–102
19. Nagai, T., Ibata, K., Park, E. S., Kubota, M., Mikoshiba, K., and Miyawaki, A. (2002) *Nat. Biotechnol.* **20,** 87–90
20. Zacharias, D. A., Violin, J. D., Newton, A. C., and Tsien, R. Y. (2002) *Science* **296,** 913–916
21. Makino, A., Baba, T., Fujimoto, K., Iwamoto, K., Yano, Y., Terada, N., Ohno, S., Sato, S. B., Ohta, A., Umeda, M., Matsuzaki, K., and Kobayashi, T. (2003) *J. Biol. Chem.* **278,** 3204–3209
22. Carmichael, J., DeGraff, W. G., Gazdar, A. F., Minna, J. D., and Mitchell, J. B. (1987) *Cancer Res.* **47,** 936–942
23. Campbell, R. E., Tour, O., Palmer, A. E., Steinbach, P. A., Baird, G. S., Zacharias, D. A., and Tsien, R. Y. (2002) *Proc. Natl. Acad. Sci. U. S. A.* **99,** 7877–7882
24. Prior, I. A., Muncke, C., Parton, R. G., and Hancock, J. F. (2003) *J. Cell Biol.* **160,** 165–170
25. Wilson, B. S., Steinberg, S. L., Liederman, K., Pfeiffer, J. R., Surviladze, Z., Zhang, J., Samelson, L. E., Yang, L.-h., Kotula, P. G., and Oliver, J. M. (2004) *Mol. Biol. Cell* **15,** 2580–2592
26. Wang, J. K., Kiyokawa, E., Verdin, E., and Trono, D. (2000) *Proc. Natl. Acad. Sci. U. S. A.* **97,** 394–399
27. Kiyokawa, E., Hashimoto, Y., Kurata, T., Sugimura, H., and Matsuda, M. (1998) *J. Biol. Chem.* **273,** 24479–24484
28. Escola, J. M., Kleijmeer, M. J., Stoorvogel, W., Griffith, J. M., Yoshie, O., and Geuze, H. J. (1998) *J. Biol. Chem.* **273,** 20121–20127
29. Kobayashi, T., Vischer, U. M., Rosnoblet, C., Lebrand, C., Lindsay, M., Parton, R. G., Kruithof, E. K., and Gruenberg, J. (2000) *Mol. Biol. Cell* **11,** 1829–1843
30. Kobayashi, T., Beuchat, M. H., Chevallier, J., Makino, A., Mayran, N., Escola, J. M., Lebrand, C., Cosson, P., and Gruenberg, J. (2002) *J. Biol. Chem.* **277,** 32157–32164
31. Kenworthy, A. K., Petranova, N., and Edidin, M. (2000) *Mol. Biol. Cell* **11,** 1645–1655
32. Glebov, O. O., and Nichols, B. J. (2004) *Nat. Cell Biol.* **6,** 238–243
33. Sanan, D. A., and Anderson, R. G. (1991) *J. Histochem. Cytochem.* **39,** 1017–1024
34. Parton, R. G., and Hancock, J. F. (2001) *Methods Enzymol.* **333,** 172–183
35. Baba, T., Ueda, H., Terada, N., Fujii, Y., and Ohno, S. (1999) *J. Histochem. Cytochem.* **47,** 637–648
36. Samelson, L. E. (2002) *Annu. Rev. Immunol.* **20,** 371–394
37. Winslow, M. M., Neilson, J. R., and Crabtree, G. R. (2003) *Curr. Opin. Immunol.* **15,** 299–307
38. Gouy, H., Deterre, P., Debre, P., and Bismuth, G. (1994) *J. Immunol.* **152,** 3271–3281
39. Lencer, W. I., Hirst, T. R., and Holmes, R. K. (1999) *Biochim. Biophys. Acta* **1450,** 177–190
40. Harder, T., and Simons, K. (1999) *Eur. J. Immunol.* **29,** 556–562
41. Kranenburg, O., and Moolenaar, W. H. (2001) *Oncogene* **20,** 1540–1546
42. Cobb, M. H. (1999) *Prog. Biophys. Mol. Biol.* **71,** 479–500
43. Qian, D., and Weiss, A. (1997) *Curr. Opin. Cell Biol.* **9,** 205–212
44. Zhang, W., Sloan-Lancaster, J., Kitchen, J., Trible, R. P., and Samelson, L. E. (1998) *Cell* **92,** 83–92
45. Nishibe, S., Wahl, M. I., Hernandez-Sotomayor, S. M., Tonks, N. K., Rhee, S. G., and Carpenter, G. (1990) *Science* **250,** 1253–1256
46. Straus, D. B., and Weiss, A. (1992) *Cell* **70,** 585–593
47. Irvin, B. J., Williams, B. L., Nilson, A. E., Maynor, H. O., and Abraham, R. T. (2000) *Mol. Cell. Biol.* **20,** 9149–9161
48. Williams, B. L., Schreiber, K. L., Zhang, W., Wange, R. L., Samelson, L. E., Leibson, P. J., and Abraham, R. T. (1998) *Mol. Cell. Biol.* **18,** 1388–1399
49. Koretzky, G. A., Picus, J., Schultz, T., and Weiss, A. (1991) *Proc. Natl. Acad. Sci. U. S. A.* **88,** 2037–2041
50. Hepler, J. R., Earp, H. S., and Harden, T. K. (1988) *J. Biol. Chem.* **263,** 7610–7619
51. Alessi, D. R., Cuenda, A., Cohen, P., Dudley, D. T., and Saltiel, A. R. (1995) *J. Biol. Chem.* **270,** 27489–27494
52. Chijiwa, T., Mishima, A., Hagiwara, M., Sano, M., Hayashi, K., Inoue, T., Naito, K., Toshioka, T., and Hidaka, H. (1990) *J. Biol. Chem.* **265,** 5267–5272
53. Hahner, L., McQuilkin, S., and Harris, R. A. (1991) *FASEB J.* **5,** 2466–2472
54. Finco, T. S., Kadlecek, T., Zhang, W., Samelson, L. E., and Weiss, A. (1998) *Immunity* **9,** 617–626
55. Shakor, A. B., Czurylo, E. A., and Sobota, A. (2003) *FEBS Lett.* **542,** 1–6
56. Gomez-Mouton, C., Abad, J. L., Mira, E., Lacalle, R. A., Gallardo, E., Jimenez-Baranda, S., Illa, I., Bernad, A., Manes, S., and Martinez, A. C. (2001) *Proc. Natl. Acad. Sci. U. S. A.* **98,** 9642–9647

57. Viola, A., Schroeder, S., Sakakibara, Y., and Lanzavecchia, A. (1999) *Science* **283,** 680–682
58. Sharma, P., Varma, R., Sarasij, R. C., Ira, Gousset, K., Krishnamoorthy, G., Rao, M., and Mayor, S. (2004) *Cell* **116,** 577–589
59. Gaus, K., Gratton, E., Kable, E. P., Jones, A. S., Gelissen, I., Kritharides, L., and Jessup, W. (2003) *Proc. Natl. Acad. Sci. U. S. A.* **100,** 15554–15559
60. Subczynski, W. K., and Kusumi, A. (2003) *Biochim. Biophys. Acta* **1610,** 231–243
61. Mills, G. B., and Moolenaar, W. H. (2003) *Nat. Rev. Cancer* **3,** 582–591
62. Franklin, R. A., Atherfold, P. A., and McCubrey, J. A. (2000) *Mol. Immunol.* **37,** 675–683
63. Ueda, Y., Hirai, S., Osada, S., Suzuki, A., Mizuno, K., and Ohno, S. (1996) *J. Biol. Chem.* **271,** 23512–23519
64. Marais, R., Light, Y., Mason, C., Paterson, H., Olson, M. F., and Marshall, C. J. (1998) *Science* **280,** 109–112
65. Carroll, M. P., and May, W. S. (1994) *J. Biol. Chem.* **269,** 1249–1256
66. Woodside, D. G., Obergfell, A., Talapatra, A., Calderwood, D. A., Shattil, S. J., and Ginsberg, M. H. (2002) *J. Biol. Chem.* **277,** 39401–39408
67. Umemori, H., Inoue, T., Kume, S., Sekiyama, N., Nagao, M., Itoh, H., Nakanishi, S., Mikoshiba, K., and Yamamoto, T. (1997) *Science* **276,** 1878–1881